Crystal Structure of Type 1 Ribonuclease H from Hyperthermophilic Archaeon *Sulfolobus tokodaii*: Role of Arginine 118 and C-Terminal Anchoring[†,‡]

Dong-Ju You,[§] Hyongi Chon,[§,||] Yuichi Koga,[§] Kazufumi Takano,[§,⊥] and Shigenori Kanaya*[,§]

Department of Material and Life Science, Graduate School of Engineering, Osaka University, 2-1 Yamadaoka, Suita, Osaka 565-0871, Japan, and CREST, JST, 2-1 Yamadaoka, Suita, Osaka 565-0871, Japan

Received May 2, 2007; Revised Manuscript Received August 8, 2007

ABSTRACT: The crystal structure of ribonuclease HI from the hyperthermophilic archaeon *Sulfolobus tokodaii* (Sto-RNase HI) was determined at 1.6 Å resolution. Sto-RNase HI exhibits not only RNase H activity but also double-stranded RNA-dependent ribonuclease (dsRNase) activity. The main-chain fold and steric configurations of the four acidic active-site residues of Sto-RNase HI are very similar to those of other type 1 RNases H. However, Arg118 of Sto-RNase HI is located at the position in which His124 of *E. coli* RNase HI, His539 of HIV-1 RNase H, and Glu188 of *Bacillus halodurans* RNase H are located. The mutation of this residue to Ala considerably reduced both the RNase H and dsRNase activities without seriously affecting substrate binding, suggesting that Arg118 is involved in catalytic function. This residue may promote product release by perturbing the coordination of the metal ion A as proposed for Glu188 of *B. halodurans* RNase H. In addition, the extreme C-terminal region of Sto-RNase HI is anchored to its core region by one disulfide bond and several hydrogen bonds. Differential scanning calorimetry measurements indicated that Sto-RNase HI is a hyperstable protein with a melting temperature of 102 °C. The mutations of the cysteine residues forming disulfide bond or elimination of the extreme C-terminal region greatly destabilized the protein, indicating that anchoring of the C-terminal tail is responsible for hyperstabilization of Sto-RNase HI.

Ribonuclease H (RNase H)[1] (EC 3.1.26.4) is an enzyme that specifically cleaves the RNA strand of RNA/DNA hybrids (*1*). The enzyme is widely present in various organisms, including bacteria, archaea, and eukaryotes (*2*). These RNases H are involved in DNA replication, repair, and transcription (*3*−*9*). Lack of the RNase H2 activity in human causes an autosomal recessive neurological disorder (*10*). RNase H is also found in viruses, mostly retroviruses, as a carboxyl-terminal domain of reverse transcriptase (RT) (*2*, *11*). This activity is required for proliferation of retroviruses and is therefore regarded as one of the targets for AIDS therapy (*12*).

RNases H have been classified into two major families, type 1 and type 2 RNases H, based on the difference in the amino acid sequences (*2*). *Escherichia coli* RNase HI, *Thermus thermophilus* RNase HI, human immunodeficiency virus type 1 (HIV-1) RNase H, Moloney murine leukemia virus (Mo-MLV) RNase H, and *Bacillus halodurans* RNase H (Bh-RNase H), for which the crystal structures are available (*13*−*20*), are members of the type 1 RNase H family. A folding motif of these proteins, termed the RNase H-fold, has been found not only in type 2 RNases H (*21*−*24*) but also in other proteins with nuclease or polynucleotidyl transferase activities, such as integrase (*25*), DNA transposase (*26*), RuvC Holliday junction resolvase (*27*), and a PIWI domain of Argonaute proteins (*28*−*30*), which is essential for RNA-induced silencing complex- (RISC-) mediated mRNA cleavage. Each of these enzymes contains three or four highly conserved acidic residues, which form the binding site of the catalytically essential divalent metal ion(s). Based on the crystal structures of the RNase H-substrate (*18*) and RNase H-product (*31*) complexes, a two-metal-ion mechanism has been proposed for the hydrolytic reaction catalyzed by RNase H. According to this mechanism, metal ion A is required for substrate-assisted nucleophile formation and product release, and metal ion B is required to destabilize the enzyme−substrate complex and thereby promote the phosphoryl transfer reaction (*32*).

Type 1 RNases H are further divided into four groups: bacterial RNases HI, eukaryotic RNases H1, the RNase H domains of RTs, and Sto-RNase HI homologues (*33*). Sto-RNase HI homologues include RNases HI from *Halobac-*

[†] This work was supported in part by a Grant-in-Aid for National Project on Protein Structural and Functional Analyses and by a Grant-in-Aid for Scientific Research on Priority Areas "Systems Genomics" from the Ministry of Education, Culture, Sports, Science, and Technology of Japan, and by an Industrial Technology Research Grant Program from the New Energy and Industrial Technology Development Organization (NEDO) of Japan.

[‡] The structure for Sto-RNase HI has been deposited in the Protein Data Bank under ID code 2EHG.

* To whom correspondence should be addressed. Tel/Fax: +81-6-6879-7938. E-mail: kanaya@mls.eng.osaka-u.ac.jp.

[§] Osaka University.

[||] Present address: Laboratory of Molecular Genetics, National Institutes of Health, Bethesda, MD 20892.

[⊥] CREST, JST.

[1] Abbreviations: RNase(s) H, ribonuclease(s) H; Sto-RNase HI, ribonuclease HI from *Sulfolobus tokodaii* strain 7; Bh-RNase H, ribonuclease H from *Bacillus halodurans*; RT, reverse transcriptase; HIV-1, human immunodeficiency virus type 1; Mo-MLV, Moloney murine leukemia virus; dsRNase, double-stranded RNA-dependent ribonuclease; DSC, differential scanning calorimetry

10.1021/bi700830f CCC: $37.00
Published on Web 09/25/2007

terium sp. NRC-1, *Sulfolobus tokodaii*, *Pyrobaculum aerophilum*, and *Streptomyces coelicolor*. The crystal structure is not available for any of these proteins. Sto-RNase HI from the hyperthermophilic and acidophilic archaeon *Sulfolobus tokodaii* strain 7 is a representative member of these RNases HI and its enzymatic properties have been well characterized (*33*). Sto-RNase HI is more closely related to retroviral RNases H than to bacterial and eukaryotic type 1 RNases H in primary structure and enzymatic properties. Like retroviral RNases H (*12*, *34*), Sto-RNase HI lacks a basic protrusion, can cleave RNA−DNA junctions, and exhibits not only the RNase H activity but also double-stranded RNA-dependent RNase (dsRNase) activity. In addition, Sto-RNase HI lacks a histidine residue, which is well conserved in various type 1 RNases H. Furthermore, Sto-RNase HI is expected to be hyperthermostable, because the optimum growth temperature of its source organism is 80 °C (*35*). Therefore, it would be informative to determine the crystal structure of Sto-RNase HI and compare it with those of other type 1 RNases H.

We have recently succeeded in crystallizing Sto-RNase HI and performed preliminary X-ray diffraction studies (*36*). In this report, we determined the crystal structure of Sto-RNase HI at 1.6 Å resolution. On the basis of this structure, we designed three mutant proteins at the active site and C-terminal tail, and we analyzed their enzymatic activities and stability. We showed that Arg118 of Sto-RNase HI functions as a substitute for the conserved histidine residue. We also showed that Sto-RNase HI is a highly thermostable protein and that anchoring of the C-terminal tail to the core region is responsible for its hyperstability.

Table 1: Data Collection and Refinement Statistics

		SeMet MAD data		
	native data	edge	peak	remote
wavelength (Å)	1.0000	0.9796	0.9793	0.973
space group	$P4_3$		$P4_3$	
unit cell (Å)				
$a = b$	39.21		38.72	
c	91.15		90.87	
resolution[a] (Å)	26.5−1.6 (1.66−1.6)		38.6−2.2 (2.28−2.2)	
observations	67 424	45 180	45 203	44 756
unique reflections	18 142	13 349	13 272	13 252
completeness[a] (%)	99.8 (100)	99.2 (94.5)	99.3 (95.6)	99.1 (95.0)
R_{merge}[a,b] (%)	4.7 (14.5)	8.8 (22.2)	8.9 (22.1)	8.7 (21.8)
avg $I/\sigma(I)$[a]	30.9 (6.8)	14.0 (2.6)	14.0 (2.7)	14.1 (2.6)

Refinement	
resolution limit (Å)	26.5-1.6
R factor[c] (R/R_{free})	19.4/21.8
no. of atoms (protein/solvent)	1180/139
rmsd.	
bond lengths (Å)	0.005
bond angles (deg)	1.0
mean B factors (Å^2)	
protein atoms	15.35
water atoms	26.42
Ramachandran plot statistics (%)	
most favored regions (%)	92.2
additional allowed regions (%)	7.8
generously allowed regions (%)	0.0

[a] Values in parentheses are for the highest resolution shell. [b] $R_{merge} = \sum|I_{hkl} - \langle I_{hkl}\rangle|/\sum I_{hkl}$, where I_{hkl} is the intensity measurement for reflection with indices hkl and $\langle I_{hkl}\rangle$ is the mean intensity for multiply recorded reflections. [c] R_{free} was calculated with 5% of the total reflections chosen randomly and omitted from refinement.

MATERIALS AND METHODS

Cells and Plasmids. *E. coli* MIC2067(DE3) [F^- λ^- IN-(*rrnD*−*rrnE*)1 *rnhA339::cat rnhB716::kam* (DE3)] (*37*) and plasmid pST0753 for overproduction of Sto-RNase HI (*36*) were constructed in our laboratory. Plasmid pET-25b was obtained from Novagen. *E. coli* MIC2067(DE3) transformants were grown in NZCYM medium (Novagen) containing 50 mg/L ampicillin and 0.1% glucose.

Crystallization. Overproduction, purification, crystallization, and preliminary crystallographic analyses of Sto-RNase HI and selenomethionine-substituted Sto-RNase HI (SeMet Sto-RNase HI) were carried out as described previously (*36*). All crystals were grown by the sitting-drop vapor-diffusion method at 4 °C. An aliquot (1.5 μL) of the protein solution (17 mg/mL) was mixed with 1 μL of the solution containing 0.1 M *N*-cyclohexyl-3′-aminopropanesulfonic acid (CAPS)−NaOH (pH 10.5) and 30% poly(ethylene glycol) (PEG) 400 as described previously (*36*).

X-ray Diffraction Data Collection and Structure Determination. X-ray diffraction data sets of the native and SeMet crystals were collected at −173 °C by use of synchrotron radiation on the BL41XU station at SPring-8. All data sets were processed with the program HKL2000 (*38*). Experimental phases were calculated by the multiwavelength anomalous diffraction (MAD) method using the data sets of SeMet crystals (Table 1). By utilization of automated methodology of the program SOLVE (*39*) with the MAD diffraction data, 3−4 Se atoms were identified in the asymmetric unit of the crystal, and these were used to obtain initial phases with an initial figure of merit (FOM) of 0.36 at 2.2 Å. Further density modification and solvent flattening in the program RESOLVE (*39*) resulted in phases with an FOM of 0.52 at 2.2 Å. The initial model (residues 2−149) was manually built by use of the program O (*40*). The final model (residues 1−149) was completed and refined by use of the programs O (*40*) and CNS (*41*) with a 1.6 Å data set collected on the native protein. Progress in the structural refinement was evaluated at each stage by the free R factor and by inspection of the stereochemical parameters calculated by the program PROCHECK (*42*). The Ramachandran plot produced by PROCHECK shows that all of the residues are in the favored region. The statistics for data collection and refinement are summarized in Table 1. The structural figures were prepared with PyMol (http://www.pymol.org).

Protein Data Bank Accession Number. The coordinates and structure factors have been deposited in the Protein Data Bank under ID code 2EHG.

Preparation of Mutant Proteins. Site-directed mutagenesis was carried out by the PCR overlap extension method (*43*). For construction of the gene encoding R118A-RNase HI, the mutagenic primers were designed to alter the codon for Arg118 (AGA) to GCG for Ala. For construction of the gene encoding C58/145A-RNase HI, the mutagenic primers were designed to alter the codons for Cys58 (TGT) and Cys145 (TGT) to GCG and GCC for Ala, respectively, and to silently alter the codon for Gly144 (GGA) to GGC. The gene encoding RNase HIΔC6 was amplified by PCR with 5′-primer 5′-ACATTACTACCATATGATAATTGGTTATTTTGACGGT-3′ and 3′-primer 5′-CTCGAATTCCTATATATCTCTTAACTTTCC-3′, where underlined bases represent an *Nde*I site for the 5′-primer and an *Eco*RI site for the

3′-primer. For these PCR reactions, plasmid pST0753 was used as a template. The amplified DNA fragments were digested with *Nde*I and *Eco*RI and ligated into the *Nde*I−*Eco*RI sites of plasmid pET-25b(+). All DNA oligomers for PCR were synthesized by Hokkaido System Science (Sapporo, Japan). The DNA sequences of the genes encoding truncated and mutant proteins were confirmed by a Prism 310 DNA sequencer (GE Healthcare).

Overproduction of the mutant proteins by use of *E. coli* MIC2067(DE3) transformants and purification of these proteins were performed as described for the wild-type protein (*36*). The purity of these mutant proteins were confirmed by SDS−15% PAGE (*44*), followed by staining with Coomassie Brilliant Blue. The protein concentration was determined from the UV absorption by use of an A_{280} value of 0.97 for the wild-type protein and 1.0 for RNase HIΔC6 for 0.1% solution (1 mg/mL). These values were calculated by using $\epsilon = 1576\ M^{-1}\ cm^{-1}$ for Tyr and $5225\ M^{-1}\ cm^{-1}$ for Trp at 280 nm (*45*). The protein concentrations of R118A-RNase HI and C58/145A-RNase HI were determined from the UV absorption with the assumption that these mutant proteins have the same absorption coefficient as that of the wild-type protein.

Enzymatic Activity. The 5′-end-labeled 12-bp RNA/DNA hybrid (1 μM) was prepared by hybridizing 5′-end-labeled 12-base RNA (5′-cggagaugacgg-3′) with 2.0 molar excess amount of the complementary 12-base DNA. For end-labeling of RNA, 6-carboxyfluorescein (6-FAM) was used. Hydrolysis of the substrate was carried out at 37 °C for 15 min in 10 mM Tris-HCl (pH 8.5) containing 5 mM $MgCl_2$, 10 mM NaCl, 1 mM 2-mercaptoethanol (2-Me), and 50 μg/mL bovine serum albumin (BSA). The hydrolysates were separated on a 20% polyacrylamide gel containing 7 M urea, detected by Typhoon 9240 Imager (Pharmacia/GE Healthcare), and identified by comparing their migration on the gel with those of the oligonucleotides generated by partial digestion of 5′-end-labeled 12-base RNA with *Crotalus atrox* phosphodiesterase (Sigma) (*46*). The 5′-end-labeled 12-bp RNA/RNA duplex was prepared as described for the 12-bp RNA/DNA hybrid. Hydrolysis of the substrate, separation of the hydrolysates on the urea gel, and their detection and identification were also carried out as described for the 12-bp RNA/DNA hybrid, except that the reaction buffer for hydrolysis contained 5 mM $MnCl_2$ instead of $MgCl_2$. One unit was defined as the amount of enzyme hydrolyzing 1 nmol of the substrate per minute at 37 °C. The specific activity was defined as the enzymatic activity per milligram of protein.

Binding Analysis of Proteins to RNA/DNA Hybrid. Binding of proteins to the substrate was analyzed on a BIAcore instrument (BIAcore). The 36-bp RNA/DNA hybrid was immobilized on the CM5 sensor chip (research grade) by the amino coupling method as described previously (*47*). The proteins were dissolved in 10 mM Tris-HCl (pH 8.0) containing 50 mM NaCl, 1 mM EDTA, 1 mM β-mercaptoethanol, and 0.005% (v/v) Tween P20 at concentrations varied from 1 to 200 μM. Samples were injected at 25 °C at a flow rate of 20 μL/min onto the sensor chip. The sensorgrams were analyzed with BIAevalution software (BIAcore). The association constant K_a was calculated from the equilibrium levels of the protein binding to the surface as described previously (*47*).

Circular Dichroic Spectra. The far-UV CD spectra were measured on a J-725 spectropolarimeter (Japan Spectroscopic) at 20 °C. The protein was dissolved in 20 mM sodium acetate (pH 5.5) at a concentration of 0.1 mg/mL. Optical path length was 2 mm. The mean residue ellipticity, θ, which has the units of degrees centimeter^2 decimole^{-1}, was calculated by using an average amino acid molecular weight of 110.

Differential Scanning Calorimetry. DSC measurements were carried out on a high-sensitivity VP-DSC controlled by the VPViewer software package (Microcal, Inc.) at a scan rate of 1 °C/min. The protein was dissolved in 20 mM glycine hydrochloride (pH 3.0) at a concentration of approximately 0.5 mg/mL. Prior to the measurements, samples were filtered through a 0.22-μm pore size membrane and then degassed in a vacuum. The reversibility of thermal denaturation was verified by reheating the samples.

RESULTS AND DISCUSSION

Crystallization and Structure Determination. Preliminary X-ray diffraction data of Sto-RNase HI have previously been obtained at SPring-8 (*36*). The structure was initially solved by means of multiple wavelength anomalous diffraction (MAD) phasing with the X-ray diffraction data of selenomethionine-labeled crystals. The polypeptide chain was traced by use of manual building in O, and the model was refined to an *R*-factor of 19.6% (*R*-free = 22.0%) using diffraction data of the native crystal at 1.6 Å resolution. Details of the data-collection statistics and refinement are summarized in Table 1.

Overall Structure. The crystal structure of Sto-RNase HI is shown in Figure 1A. The overall structure, which represents a typical RNase H-fold, consists of a central five-stranded mixed β sheet with three antiparallel (1, 2, and 3) and two parallel (4 and 5) strands and four α-helices (A, B, D, and E). In the designation of these α-helices and β strands, the terminology reported by Nowotny et al. (*18*) is used. The structures of *E. coli* RNase HI, HIV-1 RNase H (the RNase H domain of HIV-1 RT), and Bh-RNase H are shown in Figure 1B for comparative purposes. Sto-RNase HI shows amino acid sequence identities of 20.1% to *E . coli* RNase HI, 14.7% to HIV-1 RNase H, and 15.4% to Bh-RNase H. Despite these low amino acid sequence identities, Sto-RNase HI shows high structural similarity to these proteins with root-mean-square deviations (RMSDs) of 0.96 Å between Sto-RNase HI and *E. coli* RNase HI (for 121 Cα atoms), 1.15 Å between Sto-RNase HI and HIV-RNase H (for 113 Cα atoms), and 1.39 Å between Sto-RNase HI and Bh-RNase H (for 116 Cα atoms).

Catalytic Center. Asp7, Glu52, Asp76, and Asp125 form the active site of Sto-RNase HI. The corresponding residues are Asp10, Glu48, Asp70, and Asp134 for *E. coli* RNase HI; Asp443, Glu478, Asp498, and Asp549 for HIV-1 RNase H; and Asp71, Glu109, Asp132, and Asp192 for Bh-RNase H. Superposition of the active-site structures of Sto-RNase HI and HIV-1 RNase H on the cocrystal structure of Bh-RNase H with the substrate and metal cofactor indicates that the steric configurations of the active-site residues of Sto-RNase HI are very similar to those of HIV-1 RNase H and Bh-RNase H (Figure 1C). Therefore, these four acidic active-site residues probably form the metal binding sites A and B, as seen in the cocrystal structure of Bh-RNase H (*18*).

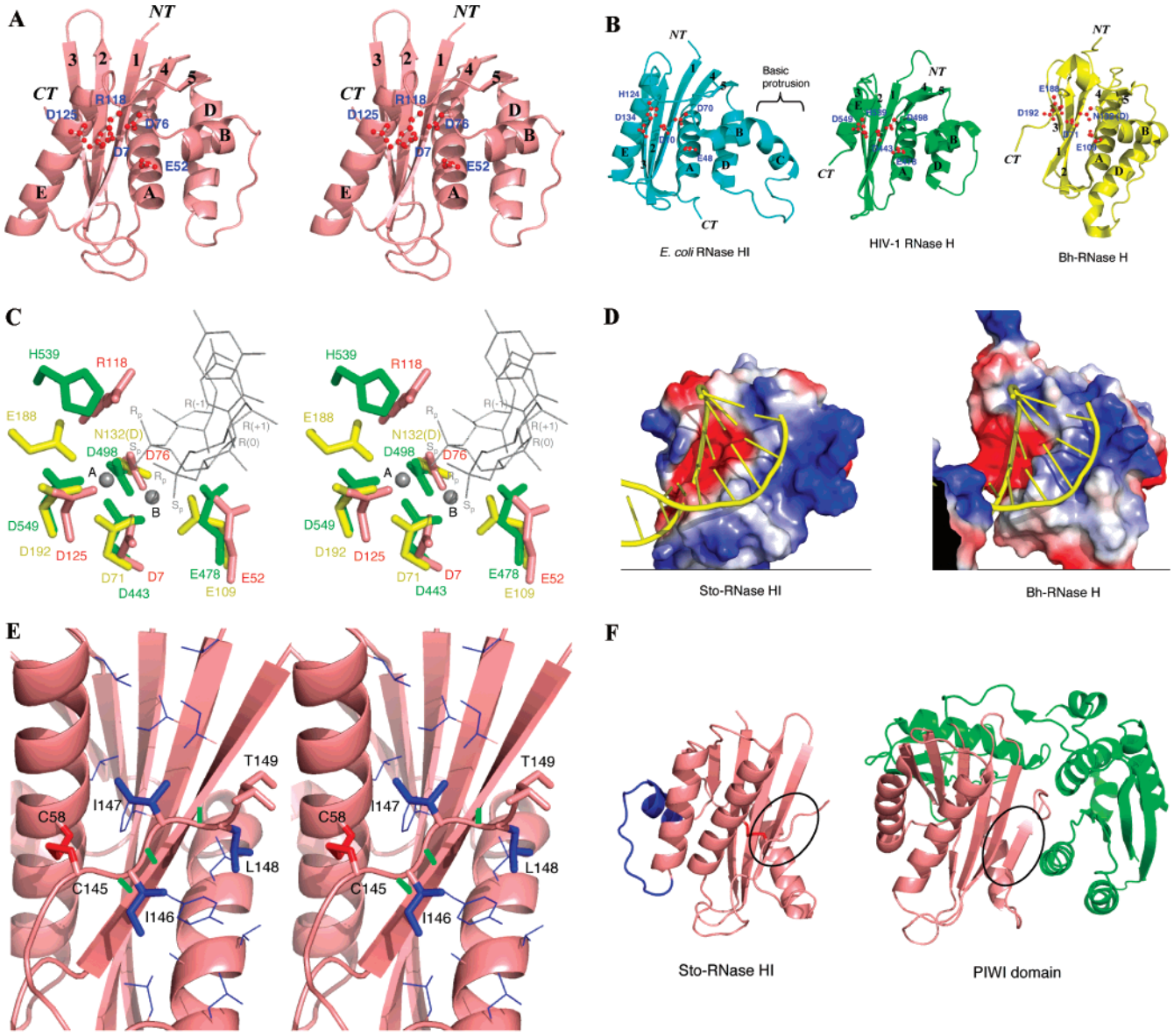

FIGURE 1: Comparison of the structures of various type 1 RNases H. (A) Stereoview of the crystal structure of Sto-RNase HI. Five active-site residues (Asp7, Glu52, Asp76, Arg118, and Asp125) are shown as red ball-and-stick models. NT and CT represents N- and C-termini. (B) Ribbon diagrams of *E. coli* RNase HI (*13*) (PDB code 1RNH), HIV-1 RNase H (*61*) (PDB code 1RTD), and Bh-RNase H (*18*) (PDB code 1ZBF). Five active-site residues are shown as red ball-and-stick models. The basic protrusion of *E. coli* RNase HI is also shown. (C) Stereoview of the active-site structures of RNases H. The side chains of the active-site residues of Sto-RNase HI (salmon) and HIV-1 RNase H (green) are superimposed onto those in the cocrystal structure of Bh-RNase H with the substrate and metal ions (yellow). The positions of the RNA strand of the substrate with the scissile phosphate group between R(−1) and R(0) and two metal ions A and B are also shown. The view direction is the same as in panels A and B. (D) Model of the Sto-RNase HI−substrate complex and cocrystal structure of Bh-RNase H with the substrate. Electrostatic surface potentials of these proteins are shown. The negative and positive potentials are shown in red and blue, respectively. The electrostatic potential value ranges from −15 to +15 kT/e. The structures of RNA/DNA hybrids are shown in yellow. The highly negatively charged region represents the active site, to which the RNA strand of RNA/DNA hybrids binds. (E) Stereoview of the structure of the C-terminal tail of Sto-RNase HI. The side chains of Cys58 and Cys145, which form the disulfide bond, are shown as red stick models. The side chains of Ile146, Ile147, and Leu148 are shown as blue stick models. The side chains of the hydrophobic residues located close to these residues are shown as thin blue stick models. The side chain of the C-terminal residue (Thr149) is also shown as a stick model. Three hydrogen bonds formed between C-terminal polypeptide chain and β3 strand are colored green. (F) Comparison of the crystal structures of Sto-RNase HI and the PIWI domain of Argonaute from *A. aeolicus* (*30*). The folding motif, which is shared by these structures, is shown in salmon. For the Sto-RNase HI structure, helix B and the loop between helices B and D are colored blue, and the disulfide bond is colored red. For the structure of the PIWI domain, the Mid/B domain is colored green. The C-terminal polypeptide chain or β strand, which is anchored to the core structure through hydrogen bonds and hydrophobic interactions, is circled. PDB code is 1YVU for *A. aeolicus* PIWI protein.

Like other Sto-RNase HI homologues, Sto-RNase HI lacks a histidine residue, which is well conserved in various type 1 RNases H. Mutation of this residue (His124 for *E. coli* RNase HI and His539 for HIV-1 RNase H) greatly reduces the enzymatic activity (*48*, *49*). Bh-RNase H also lacks this histidine residue but has Glu188 at a similar position. This residue has been proposed to promote product release by perturbing the coordination of the metal ion A (*31*), suggesting that the conserved histidine residues of type 1 RNases H play a similar role. Interestingly, Arg118 of Sto-RNase HI is located at a similar position, in which His539 of HIV-1 RNase H and Glu188 of Bh-RNase H are located (Figure

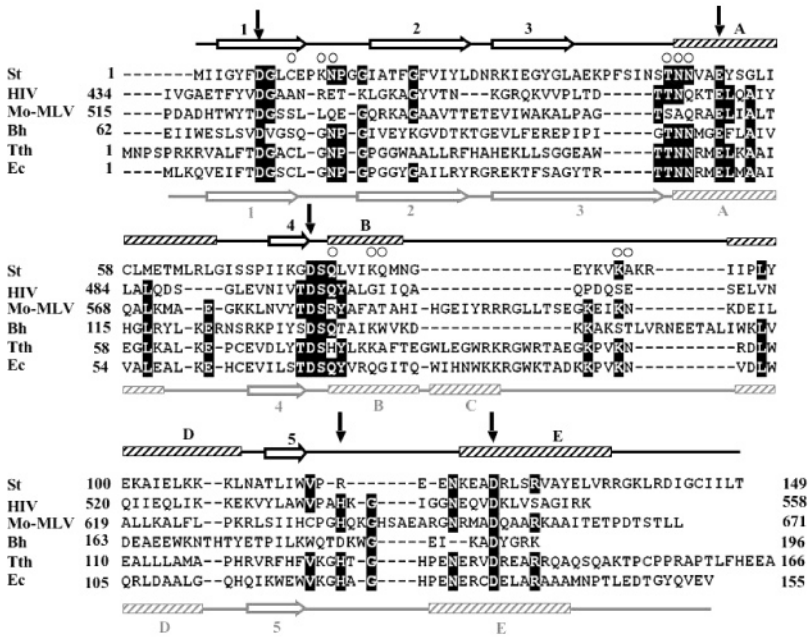

FIGURE 2: Alignment of the amino acid sequences. Sequences of Sto-RNase HI (St), HIV-1 RNase H (HIV), Mo-MLV RNase H (Mo-MLV), Bh-RNase H (Bh), *T. thermophilus* RNase HI (Tth), and *E. coli* RNase HI (Ec) are compared with one another on the basis of their crystal structures. Secondary structures of Sto-RNase HI and *E. coli* RNase HI are shown above and below the sequences, respectively. The amino acid residues that are conserved in at least four different proteins are highlighted in black. The positions of the five active-site residues are indicated by arrows. The 11 amino acid residues that contact the substrate in the cocrystal structure of Bh-RNase H with the substrate are indicated by an open circle above the sequence. Gaps are denoted by dashes. The numbers represent the positions of the amino acid residues relative to the initiator methionine for each protein.

1C). His124 of *E. coli* RNase HI is also located at a similar position according to the structure of Yang et al. (*14*) (data not shown).

Substrate-Binding Site. According to the cocrystal structure of Bh-RNase H with the substrate (*18*), Ser74, Gly76, Glu109, Asp132, and Gln134 directly contact the five consecutive 2′-OH groups of the RNA strand. Asn106 indirectly contacts the 2′-OH group immediately 5′ to the scissile phosphate group through a water molecule. Of these, Ser74 and Gly76 are replaced by Cys10 and Lys13, while Asn106, Glu109, Asp132, and Gln134 are conserved as Asn49, Glu52, Asp76, and Gln78 in Sto-RNase HI, respectively (Figure 2). Ser74 and Gly76 form hydrogen bonds with the 2′-OH group of RNA through main-chain carbonyl oxygen and amide proton atoms, respectively. Therefore, replacement of these residues with other residues may not seriously affect the interaction between the protein and substrate, unless the backbone structure is significantly changed. These results suggest that the binding site of Bh-RNase H for the RNA strand of RNA/DNA hybrids is well conserved in Sto-RNase HI. In addition, Asn77 and Asn105, which donate hydrogen bonds to bases in the minor groove, are conserved as Asn14 and Asn48 in Sto-RNase HI, respectively (Figure 2).

In contrast, the DNA binding site, which consists of the N-terminus of αA helix and the loops between αB and αD helices and between β1 and β2 strands, is not well conserved in Sto-RNase HI. In Bh-RNase H, Thr104, Asn106, Ser147, and Thr148 directly contact the DNA backbone phosphate two bases away from the scissile phosphate group. Lys138 and Trp139 indirectly and directly contact the DNA backbone phosphate three bases away from the scissile phosphate group, respectively. Of these residues, Thr104, Asn106, and Lys138 are conserved as Thr47, Asn49, and Lys82, while Trp139, Ser147, and Thr148 are replaced by Gln83, Lys91, and Ala92 in Sto-RNase HI, respectively (Figure 2). Because these sites are expected to play a key role in anchoring the B-form DNA and contribute to the specificity for an RNA/DNA hybrid, weak conservation of these sites may account for the capability of Sto-RNase HI to cleave dsRNA. Alternatively, it may account for the difference in the cleavage site specificities of Bh-RNase H and Sto-RNase HI. Weaker conservation of the DNA binding site as compared to that of the RNA binding site is also observed in HIV-1 and Mo-MLV RNases H (Figure 2), which can cleave both RNA/DNA hybrids and dsRNA (*34*, *50*). It has been reported that one of the active-site mutants of Sto-RNase HI (D125N) retains the RNase H activity but not the dsRNase activity (*33*). We also found that mutation of Lys91 of Sto-RNase HI to Ala significantly reduces the dsRNase activity without seriously affecting the RNase H activity (D.-J. You, personal communication). Similar results have been reported for Mo-MLV RNase H, although two types of mutants, which show opposite phenotypes, can be obtained (*50*). One exhibits only the RNase H activity, while the other exhibits only the dsRNase activity. These results suggest that a subtle conformational change around the substrate binding site is sufficient to alter the substrate specificity of Sto-RNase H. Further mutational and structural studies will be required to understand the mechanism by which Sto-RNase HI can recognize both RNA/DNA hybrid and dsRNA as a substrate.

Like HIV-RNase H and Bh-RNase H, Sto-RNase HI lacks helix C and the following loop, which are present as a basic protrusion in *E. coli* RNase HI (Figure 1A,B). This basic protrusion has been shown to be important for substrate binding (*47*, *51*). In the Sto-RNase HI structure, however, several basic residues, such as Lys89, Lys91, and Lys93, are clustered in a position where this basic protrusion is

present. The basic residues are also clustered in a similar position in Bh-RNase H but not in HIV-1 RNase H. In HIV-1 RNase H, the polymerase domain of RT functions as a substitute for the basic protrusion. When a model for the complex between Sto-RNase HI and substrate is constructed and the electrostatic potentials on the solvent-accessible surface area are displayed, the binding sites of the RNA and DNA strands of RNA/DNA hybrids are negatively and positively charged, respectively, as in the cocrystal structure of Bh-RNase H with the substrate (Figure 1D). These results suggest that electrostatic interactions contribute to the substrate binding.

C-Terminal Tail. When the crystal structures of Sto-RNase HI, *E. coli* RNase HI, HIV-1 RNase H, and Bh-RNase H are compared with one another, significant differences are observed at the C-terminal region (Figure 1A,B). The C-terminal regions of Sto-RNase HI and *E. coli* RNase HI are characterized by the presence of a long helix (helix E) and a long tail. HIV-1 RNase H has a short helix E and a short tail. Bh-RNase H has a long tail but lacks helix E. While the C-terminal tails of *E. coli* RNase HI, HIV-1 RNase H, and Bh-RNase H are almost fully exposed to the solvent, that of Sto-RNase HI is anchored to the core region through a disulfide bond, hydrogen bonds, and hydrophobic interactions (Figure 1E). The disulfide bond is formed between Cys58, which is located at the middle of helix A, and Cys145. The hydrogen bonds are formed between the main chain at Ile146−Leu148 and main chain of the β3 strand. The side chains of Ile146, Ile147, and Leu148 make hydrophobic interactions with the core region. These results suggest that anchoring of the C-terminal tail contributes to the stabilization of Sto-RNase HI.

It is noted that the structure of Sto-RNase HI is highly similar to that of the RNase H-like domain of the PIWI domain of Argonaute from *Aquifex aiolicus*, especially in the C-terminal region (Figure 1F). Unlike other Argonaute proteins, *A. aeolicus* Argonaute exhibits both RNA-guided and DNA-guided RNase activities, using the RNase H-like domain of the PIWI domain (*30*). According to the crystal structure of *A. aeolicus* PIWI protein, a part of the C-terminal tail behind helix E forms the β6 strand, which is hydrogen-bonded to the β3 strand to form a large six-stranded β-sheet stabilized by hydrophobic interactions (*30*). The corresponding polypeptide chain is hydrogen-bonded to β3 strand but does not form a β strand in the Sto-RNase H structure, probably because the position of this polypeptide chain is shifted upon formation of the disulfide bond, such that it is unfavorable for the formation of a β strand.

Effect of Mutation of Arg118. To analyze the role of Arg118 of Sto-RNase HI, the mutant protein R118A-RNase HI was constructed. The far-UV CD spectrum of this mutant protein was nearly identical to that of the wild-type protein (data not shown), suggesting that the protein structure is not markedly changed by the mutation. The RNase H and dsRNase activities of R118A-RNase HI were determined by use of the 12-bp RNA/DNA and RNA/RNA substrates in the presence of 5 mM $MgCl_2$ and $MnCl_2$, respectively, and compared with those of the wild-type protein. Ohtani et al. (*33*) have previously reported that Sto-RNase HI exhibited maximal RNase H and dsRNase activities in the presence of 1 mM $MgCl_2$ and $MnCl_2$, respectively. However, they analyzed these activities only in the presence of 0.1, 1, and 10 mM $MgCl_2$ or $MnCl_2$. When the Sto-RNase HI activities were analyzed in the presence of 0.005, 0.05, 0.5 1, 5, and 10 mM $MgCl_2$ or $MnCl_2$ under the same conditions as reported previously, Sto-RNase HI exhibited maximal RNase H and dsRNase activities in the presence of 5 mM $MgCl_2$ and 5 mM $MnCl_2$, respectively (data not shown). Sto-RNase HI cleaved both the RNA/DNA and RNA/RNA substrates at multiple sites as reported previously (*33*), while R118A-RNase HI poorly cleaved these substrates (Figure 3). The specific activities of R118A-RNase HI for both substrates were reduced by approximately 10-fold as compared to those of the wild-type protein (Table 2).

To examine whether mutation of Arg118 affects the substrate binding, interactions of the wild-type and mutant proteins with the 36-bp RNA/DNA hybrid were analyzed by BIAcore (Figure 4). The association constants (K_a) of these proteins, estimated from the equilibrium binding level to the substrate, were 3.81×10^4 for the wild-type protein and 1.09×10^4 for R118A-RNase HI, indicating that the association constant of R118A-RNase HI was reduced by 3.5-fold as compared to that of the wild-type protein. These results suggest that the mutation of Arg118 affects the catalytic function more seriously than the substrate binding. Arg118 may promote product release by perturbing the coordination of the metal ion A, as proposed for Glu188 of Bh-RNase H, although Arg118 and Glu188 are oppositely charged in normal conditions. Glu188 may perturb the coordination of the metal ion A by making a direct coordination with this metal ion, while Arg118 may perturb it by electrostatic interactions.

The association constants of other RNases H for the interaction with the same 36-bp RNA/DNA hybrid have been reported to be 4.7×10^7 for *E. coli* RNase HI (*47*) and 1.9×10^8 for *Bacillus stearothermophilus* RNase HIII (*24*), indicating that the association constant of Sto-RNase HI is 3−4 orders of magnitude lower than those of *E. coli* RNase HI and *B. stearothermophilus* RNase HIII. Lack of the basic protrusion or the substrate binding domain may account for the extremely weak binding of Sto-RNase HI to the substrate. It is noted that the interaction between protein and substrate was analyzed in the absence of the metal cofactor. The binding affinity of Sto-RNase HI for the substrate may increase in the presence of the metal cofactor, because the negative charge repulsion between protein and substrate may be reduced when the metal cofactor binds to the active site. It is also noted that interaction between Sto-RNase HI and substrate was analyzed by use of the 36-bp RNA/DNA hybrid instead of the 12-bp RNA/DNA hybrid. Because Sto-RNase HI nonspecifically cleaves the substrate at multiple sites, it is highly expected that the specific activity of R118A-RNase HI relative to that of wild-type protein is not seriously changed regardless of whether the 12- or 36-bp RNA/DNA hybrid is used as a substrate. In fact, the specific activity of R118A-RNase HI for hydrolysis of the polymeric substrate, M13 DNA/RNA hybrid, was also decreased by approximately 10-fold as compared to that of wild-type protein (D.-J. You, personal communication).

Effect of Mutation at the C-Terminal Region. To examine whether anchoring of the C-terminal tail contributes to the stabilization of Sto-RNase HI, two mutant proteins, C58/145A-RNase HI and RNase HIΔC6, were constructed. C58/145A-RNase HI lacks the disulfide bond, and RNase HIΔC6

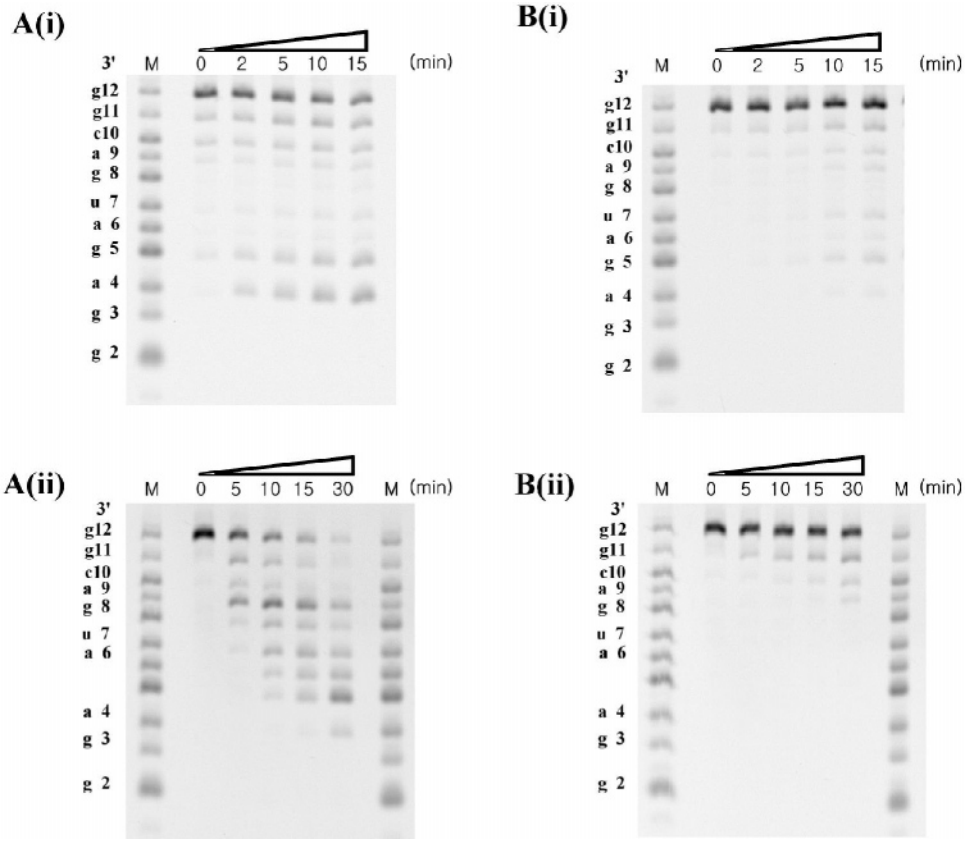

FIGURE 3: RNase H and dsRNase activities of Sto-RNase HI and its mutants. The 12-bp RNA/DNA hybrid (i) and RNA/RNA duplex (ii) were incubated with Sto-RNase HI (A) and R118A-RNase HI (B) at 37 °C, and hydrolyses of these substrates were analyzed by polyacrylamide gel electrophoresis, as described under Materials and Methods. The reaction time is indicated above each lane. The reaction buffer was 10 mM Tris-HCl (pH 8.5) containing 5 mM $MgCl_2$ (for RNase H) or $MnCl_2$ (for dsRNase), 10 mM NaCl, 1 mM 2-Me, and 50 μg/mL BSA. The concentration of the substrate was 1.0 μM, and the concentration of the protein was 20 and 150 nM for hydrolyses of the RNA/DNA hybrid and RNA/RNA duplex, respectively. M represents the partial digests of the 12-base RNA with *C. atrox* phosphodiesterase.

Table 2: RNase H and dsRNase Activities of the Mutant Proteins[a]

	RNase H		dsRNase	
protein activity	specific activity (units/mg)	relative activity (%)	specific activity (units/mg)	relative activity (%)
wild type	120	100	21	100
R118A-RNase HI	9.2	7.7	2.5	12
C58/145A-RNase HI	140	120	26	120
RNase HIΔC6	93	78	12	57

[a] The RNase H and dsRNase activities were determined at 37 °C by use of the 12-bp RNA/DNA and RNA/RNA substrates in the presence of 5 mM $MgCl_2$ and $MnCl_2$, respectively, as described under Materials and Methods. Each experiment was carried out at least twice, and the average value is shown. Errors are within 20% of the values reported.

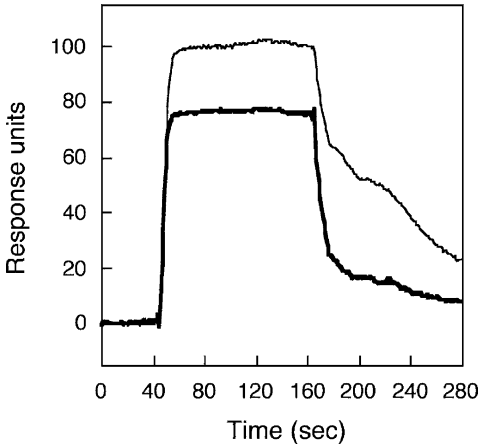

FIGURE 4: Sensorgrams from BIAcore showing the binding of Sto-RNase HI (thin line) and R118A-RNase HI (thick line) to immobilized 36-bp RNA/DNA hybrid. The protein concentration was 100 μM. Injections were done at 40 s for 120 s.

lacks the C-terminal six residues. The far-UV CD spectra of these mutant proteins were nearly identical to that of wild-type protein (data not shown), suggesting that the protein structure is not markedly changed by these mutations. Both mutant proteins were enzymatically active, because they exhibited both RNase H and dsRNase activities (Table 2). The RNase H and dsRNase activities of C58/145A-RNase HI were slightly higher than, but comparable to, those of wild-type protein, while these activities of RNase HIΔC6 were reduced by 20−40% as compared to those of wild-type protein, suggesting that the conformation of the active site and/or substrate binding site is slightly altered by the C-terminal truncation. The cleavage-site specificities of both mutant proteins were nearly identical to those of wild-type protein (data not shown).

Heat-induced unfolding of Sto-RNase HI, C58/145A-RNase HI, and RNase HIΔC6 was analyzed by differential scanning calorimetry (DSC) at pH 3.0 (Figure 5). All DSC curves were reproduced by repeating thermal scans, indicating that thermal unfolding of these proteins is reversible. The denaturation curves of all proteins showed single transitions. The peak of this curve represents the melting

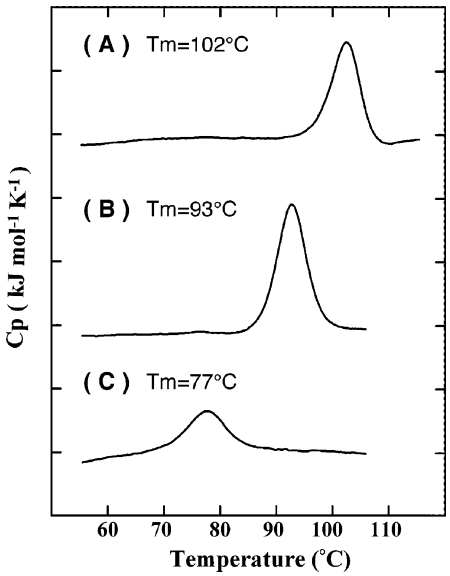

FIGURE 5: DSC curves of Sto-RNase HI and its mutants. The DSC curves of Sto-RNase HI (A), C58/145A-RNase HI (B), and RNase HIΔC6 (C), which were measured at a scan rate of 1 °C/min, are shown. These proteins were dissolved in 20 mM glycine hydrochloride (pH 3.0) at approximately 0.5 mg/mL. The increments in excess heat capacity are 50 kJ mol^{-1} K^{-1}.

temperature (T_m) of the protein, which was 102 °C for the wild-type protein, 93 °C for C58/145A-RNase HI, and 78 °C for RNase HIΔC6. These results indicate that Sto-RNase HI is a hyperthermostable protein, with a T_m value beyond the boiling temperature, and is destabilized by elimination of the disulfide bond and C-terminal truncation by 9 and 24 °C in T_m, respectively. Because C-terminal truncation not only eliminates hydrogen bonds and hydrophobic interactions but also eliminates the disulfide bond, hydrogen bonds and hydrophobic interactions contributes to the stabilization of the protein by 15 °C in T_m. Formation of the disulfide bond contributes to it by 9 °C in T_m. Of various type 1 RNases H, *T. thermophilus* RNase HI has been used as a model protein to analyze the stabilization mechanism of thermophilic proteins (*52*). The C-terminal 14 residues of this protein are structurally disordered (*15*), suggesting that the C-terminal tail is not anchored to the core region. The T_m value of *T. thermophilus* RNase HI has been reported to be 86 °C (*52*). Because the stability of RNase HIΔC6 is comparable to that of *T. thermophilus* RNase HI, anchoring of the C-terminal tail is a major factor responsible for hyperstabilization of Sto-RNase HI.

Other Structural Features for Thermostabilization of Sto-RNase HI. It has been reported that hyperthermophilic proteins are stabilized by various factors, including increased number of ion pairs (*53*, *54*), higher core hydrophobicity (*55*), increased packing density (*56*), and shorter surface loops (*57*). It has also been reported that stabilization strategies vary for different hyperthermophilic proteins, even for the same family proteins (*58*, *59*), and combination of these strategies increase the denaturation temperature of the protein up to 150 °C (*60*). To examine whether these factors also contribute to the stabilization of Sto-RNase HI, the contents of the surface charged and buried apolar residues, number of ion pairs, and number of disulfide bonds of Sto-RNase HI are compared with those of *E. coli* and *T. thermophilus* RNases HI. The results indicate that none of them correlate with the protein stability (Table 3). For example, the content of surface charged residues and number of ion pairs increases as the protein stability increases for *E. coli* and *T. thermophilus* RNases HI but rather decreases as the protein stability increases for *T. thermophilus* RNase HI and Sto-RNase HI. Likewise, the content of the buried apolar residues decreases as the protein stability increases for *E. coli* and *T. thermophilus* RNases HI but increases as the protein stability increases for *T. thermophilus* RNase HI and Sto-RNase HI. In addition, only Sto-RNase HI has the intramolecular disulfide bond. These results suggest that Sto-RNase HI is stabilized by the combination of increased core hydrophobicity, increased compactness, and disulfide bond formation. The Sto-RNase HI structure is more compact than the *E. coli* RNase HI and *T. thermophilus* RNase HI structures, because it lacks the basic protrusion and C-terminal extension as mentioned above.

Table 3: Structural Features of Mesophilic and Thermophilic RNases HI

	E. coli RNase HI	*T. thermophilus* RNase HI	Sto-RNase HI
no. of amino acids	155	166	149
T_m (°C)	66[a]	86[a]	102
content of residues (%)			
surface charged	42	46	45
buried apolar	48	43	51
no. of ion pairs (≤5.0 Å)	10	15	11
no. of disulfide bonds	0	0	1

[a] Data from Robic et al. (*52*).

ACKNOWLEDGMENT

The synchrotron radiation experiments were performed at the beam line BL41XU and BL44XU in the SPring-8 with the approval of the Japan Synchrotron Radiation Research Institute (JASRI) (2005B1766 and 2006A2733), and of Institute for Protein Research, Osaka University (2005B6709 and 2006A6812). We thank Drs. H. Matsumura, T. Inoue, and Y. Kai for their support in X-ray crystallography and helpful discussions.

REFERENCES

1. Crouch, R. J., and Dirksen, M. L. (1982) Ribonuclease H, in *Nuclease* (Linn, S. M., and Robert, R. J., Eds.) pp 211−241, Cold Spring Harbor Laboratory Press, Cold Spring Harbor, NY.
2. Ohtani, N., Haruki, M., Morikawa, M., and Kanaya, S. (1999) Molecular Diversities of RNase H, *J. Biosci. Bioeng. 88*, 12−19.
3. Kogoma, T., and Foster, P. L. (1998) Physiological functions of *E. coli* RNase HI, In *Nuclease* (Linn, S. M., and Robert, R. J., Eds.) pp 211−241, Cold Spring Harbor Laboratory Press, Cold Spring Harbor, NY.
4. Itaya, M., Omori, A., Kanaya, S., Crouch, R. J., Tanaka, T., and Kondo, K. (1999) Isolation of RNase H genes that are essential for growth of *Bacillus subtilis* 168, *J. Bacteriol. 181*, 2118−2123.
5. Qiu, J., Qian, Y., Frank, P., Wintersberger, U., and Shen, B. (1999) *Saccharomyces cerevisiae* RNase H(35) functions in RNA primer removal during lagging-strand DNA synthesis, most efficiently in cooperation with Rad27 nuclease, *Mol. Cell. Biol. 19*, 8361−8371.
6. Arudchandran, A., Cerritelli, S., Narimatsu, S., Itaya, M., Shin, D. Y., Shimada, Y., and Crouch, R. J. (2000) The absence of ribonuclease H1 or H2 alters the sensitivity of *Saccharomyces cerevisiae* to hydroxyurea, caffeine and ethyl methanesulphonate: implications for roles of RNases H in DNA replication and repair, *Genes Cells 5*, 789−802.
7. Haruki, M., Tsunaka, Y., Morikawa, M., and Kanaya, S. (2002) Cleavage of a DNA-RNA-DNA/DNA chimeric substrate contain-

ing a single ribonucleotide at the DNA-RNA junction with prokaryotic RNases HII, *FEBS Lett. 531*, 204−208.
8. Rydberg, B., and Game, J. (2002) Excision of misincorporated ribonucleotides in DNA by RNase H (type 2) and FEN-1 in cell-free extracts, *Proc. Natl. Acad. Sci. U.S.A. 99*, 16654−16659.
9. Cerritelli, S. M., Frolova, E. G., Feng, C., Grinberg, A., Love, P. E., and Crouch, R. J. (2003) Failure to produce mitochondrial DNA results in embryonic lethality in *Rnaseh1* null mice, *Mol. Cell 11*, 807−815.
10. Crow, Y. J., Leitch, A., Hayward, B. E., Garner, A., Parmar, R., Griffith, E., Ali, M., Semple, C., Aicardi, J., Babul-Hirji, R., Baumann, C., Baxter, P., Bertini, E., Chandler, K. E., Chitayat, D., Cau, D., Dery, C., Fazzi, E., Goizet, C., King, M. D., Klepper, J., Lacombe, D., Lanzi, G., Lyall, H., Martinez-Frias, M. L., Mathieu, M., McKeown, C., Monier, A., Oade, Y., Quarrell, O. W., Rittey, C. D., Rogers, R. C., Sanchis, A., Stephenson, J. B., Tacke, U., Till, M., Tolmie, J. L., Tomlin, P., Voit, T., Weschke, B., Woods, C. G., Lebon, P., Bonthron, D. T., Ponting, C. P., and Jackson, A. P. (2006) Mutations in genes encoding ribonuclease H2 subunits cause Aicardi-Goutieres syndrome and mimic congenital viral brain infection, *Nat. Genet. 38*, 910−916.
11. Radziwill, G., Tucker, W., and Schaller, H. (1990) Mutational analysis of the hepatitis B virus P gene product: domain structure and RNase H activity, *J. Virol. 64*, 613−620.
12. Hughes, S. H., Arnold, E., and Hostomsky, Z. (1998) RNase H of retroviaral reverse transcriptase, in *Nuclease* (Linn, S. M., and Robert, R. J., Eds.) pp 211−241, Cold Spring Harbor Laboratory Press, Cold Spring Harbor, NY.
13. Katayanagi, K., Miyagawa, M., Matsushima, M., Ishikawa, M., Kanaya, S., Ikehara, M., Matsuzaki, T., and Morikawa, K. (1990) Three-dimensional structure of ribonuclease H from *E. coli*, *Nature 347*, 306−309.
14. Yang, W., Hendrickson, W. A., Crouch, R. J., and Satow, Y. (1990) Structure of ribonuclease H phased at 2 Å resolution by MAD analysis of the selenomethionyl protein, *Science 249*, 1398−1405.
15. Ishikawa, K., Okumura, M., Katayanagi, K., Kimura, S., Kanaya, S., Nakamura, H., and Morikawa, K. (1993) Crystal structure of ribonuclease HI from *Thermus thermophilus* HB8 refined at 2.8 Å resolution, *J. Mol. Biol. 230*, 529−542.
16. Davies, J. F., Hostomska, Z., Hostomsky, Z., Jordan, S. R., and Matthews, D. A. (1991) Crystal structure of the ribonuclease H domain of HIV-1 reverse transcriptase, *Science 252*, 88−95.
17. Kohlstaedt, L. A., Wang, J., Friedman, J. M., Rice, P. A., and Steitz, T. A. (1992) Crystal structure at 3.5 Å resolution of HIV-1 reverse transcriptase complexed with an inhibitor, *Science 256*, 1783−1790.
18. Nowotny, M., Gaidamakov, S. A., Crouch, R. J., and Yang, W. (2005) Crystal Structures of RNase H Bound to an RNA/DNA Hybrid: Substrate Specificity and Metal-Dependent Catalysis, *Cell 121*, 1005−1016.
19. Lim, D., Gregorio, G. G., Bingman, C., Martinez-Hackert, E., Hendrickson, W. A., and Goff, S. P. (2006) Crystal structure of the moloney murine leukemia virus RNase H domain, *J. Virol. 80*, 8379−8389.
20. Das, D., and Georgiadis, M. M. (2004) The crystal structure of the monomeric reverse transcriptase from Moloney murine leukemia virus, *Structure 12*, 819−829.
21. Lai, L., Yokota, H., Hung, L. W., Kim, R., and Kim, S. H. (2000) Crystal structure of archaeal RNase HII: a homologue of human major RNase H, *Structure 8*, 897−904.
22. Muroya, A., Tsuchiya, D., Ishikawa, M., Haruki, M., Morikawa, M., Kanaya, S., and Morikawa, K. (2001) Catalytic center of an archaeal Type 2 Ribonuclease H as revealed by X-ray crystallographic and mutational analyses, *Protein Sci. 10*, 707−714.
23. Chapados, B. R., Chai, Q., Hosfield, D. J., Shen, B., and Tainer, J. A. (2001) Structural biochemistry of a type 2 RNase H: RNA primer recognition and removal during DNA replication, *J. Mol. Biol. 307*, 541−556.
24. Chon, H., Matsumura, H., Koga, Y., Takano, K., and Kanaya, S. (2006) Crystal structure and structure-based mutational analyses of RNase HIII from *Bacillus stearothermophilus*: a new Type 2 RNase H with TBP-like substrate-binding domain at the N-terminus, *J. Mol. Biol. 356*, 165−178.
25. Dyda, F., Hickman, A. B., Jenkins, T. M., Engelman, A., Craigie, R., and Davies, D. R. (1994) Crystal structure of the catalytic domain of HIV-1 integrase: similarity to other polynucleotidyl transferases, *Science 266*, 1981−1986.
26. Rice, P., and Mizuuchi, K. (1995) Structure of the bacteriophage Mu transposase core: a common structural motif for DNA transposition and retroviral integration, *Cell 82*, 209−220.
27. Ariyoshi, M., Vassylyev, D. G., Iwasaki, H., Nakamura, H., Shinagawa, H., and Morikawa, K. (1994) Atomic structure of the RuvC resolvase: a holliday junction-specific endonuclease from *E. coli*, *Cell 78*, 1063−1072.
28. Song, J. J., Smith, S. K., Hannon, G. J., and Joshua-Tor, L. (2004) Crystal structure of Argonaute and its implications for RISC slicer activity, *Science 305*, 1434−1437.
29. Parker, J. S., Roe, S. M., and Barford, D. (2005) Structural insights into mRNA recognition from a PIWI domain-siRNA guide complex, *Nature 434*, 663−666.
30. Yuan, Y. R., Pei, Y., Ma, J. B., Kuryavyi, V., Zhadina, M., Meister, G., Chen, H. Y., Dauter, Z., Tuschl, T., and Patel, D. J. (2005) Crystal structure of *A. aeolicus* Argonaute, a site-specific DNA-guided endoribonuclease, provides insights into RISC-mediated mRNA cleavage, *Mol. Cell. 19*, 405−419.
31. Nowotny, M., and Yang, W. (2006) Stepwise analyses of metal ions in RNase H catalysis from substrate destabilization to product release, *EMBO J. 25*, 1924−1933.
32. Yang, W., Lee, J. Y., and Nowotny, M. (2006) Making and breaking nucleic acids: two-Mg^{2+}-ion catalysis and substrate specificity, *Mol. Cell 22*, 5−13.
33. Ohtani, N., Yanagawa, H., Tomita, M., and Itaya, M. (2004) Cleavage of double-stranded RNA by RNase HI from a thermoacidophilic archaeon, *Sulfolobus tokodaii* 7, *Nucleic Acids Res. 32*, 5809−5819.
34. Gotte, M., Maier, G., Onori, A. M., Cellai, L., Wainberg, M. A., and Heumann, H. (1999) Temporal coordination between initiation of HIV (+)-strand DNA synthesis and primer removal, *J. Biol. Chem. 274*, 11159−11169.
35. Suzuki, T., Iwasaki, T., Uzawa, T., Hara, K., Nemoto, N., Kon, T., Ueki, T., Yamagishi, A., and Oshima, T. (2002) *Sulfolobus tokodaii* sp. nov. (f. *Sulfolobus sp. strain 7*), a new member of the genus *Sulfolobus* isolated from Beppu Hot Springs, Japan, *Extremophiles 6*, 39−44.
36. You, D.-J., Chon, H., Koga, Y., Takano, K., and Kanaya, S. (2006) Crystallization and preliminary crystallographic analysis of Type 1 RNase H from hyperthermophilic archaeon *Sulfolobus tokodaii* 7, *Acta Crystallogr. F 62*, 781−784.
37. Ohtani, N., Haruki, M., Muroya, A., Morikawa, M., and Kanaya, S. (2000) Characterization of ribonuclease HII from *Escherichia coli* overproduced in a soluble form, *J. Biochem. (Tokyo) 127*, 895−899.
38. Otwinowski, Z., and Minor, W. (1997) Processing of X-ray diffraction data collected in oscillation mode, *Methods Enzymol. 276*, 307−326.
39. Terwilliger, T. (2004) SOLVE and RESOLVE: automated structure solution, density modification and model building, *J. Synchrotron Radiat. 11*, 49−52.
40. Jones, T. A., Zou, J. Y., Cowan, S. W., and Kjeldgaard, M. (1991) Improved methods for building protein models in electron density maps and the location of errors in these models, *Acta Crystallogr. A 47*, 110−119.
41. Brunger, A. T., Adams, P. D., Clore, G. M., DeLano, W. L., Gros, P., Grosse-Kunstleve, R. W., Jiang, J. S., Kuszewski, J., Nilges, M., Pannu, N. S., Read, R. J., Rice, L. M., Simonson, T., and Warren, G. L. (1998) Crystallography and NMR system: A new software suite for macromolecular structure determination, *Acta Crystallogr. D 54*, 905−921.
42. Laskowski, R. A., MacArthur, M. W., Moss, D. S., and Thornton, J. M. (1993) PROCHECK: a program to check the stereochemical quality of protein structures, *J. Appl. Crystallogr. 26*, 283−291.
43. Horton, R. M., Cai, Z. L., Ho, S. N., and Pease, L. R. (1990) Gene splicing by overlap extension: tailor-made genes using the polymerase chain reaction, *BioTechniques 8*, 528−535.
44. Laemmli, U. K. (1970) Cleavage of structural proteins during the assembly of the head of bacteriophage T4, *Nature 227*, 680−685.
45. Goodwin, T. W., and Morton, R. A. (1946) The spectrophotometric determination of tyrosine and tryptophan in proteins, *Biochem. J. 40*, 628−632.
46. Jay, E., Bambara, R., Padmanabham, P., and Wu, R. (1974) DNA sequence analysis: a general, simple and rapid method for sequencing large oligodeoxyribonucleotide fragments by mapping, *Nucleic Acids Res. 1*, 331−353.

47. Haruki, M., Noguchi, E., Kanaya, S., and Crouch, R. J. (1997) Kinetic and stoichiometric analysis for the binding of *Escherichia coli* ribonuclease HI to RNA-DNA hybrids using surface plasmon resonance, *J. Biol. Chem. 272*, 22015−22022.
48. Oda, Y., Yoshida, M., and Kanaya, S. (1993) Role of histidine 124 in the catalytic function of ribonuclease HI from *Escherichia coli*, *J. Biol. Chem. 268*, 88−92.
49. Schatz, O., Cromme, F. V., Gruninger-Leitch, F., and Le, Grice, S. F. J. (1989) Point mutations in conserved amino acid residues within the C-terminal domain of HIV-1 reverse transcriptase specifically repress RNase H function, *FEBS Lett. 257*, 311−314.
50. Blain, S. W., and Goff, S. P. (1993) Nuclease activities of Moloney murine leukemia virus reverse transcriptase. Mutants with altered substrate specificities, *J. Biol. Chem. 268*, 23585−23592.
51. Kanaya, S., Katsuda-Nakai, C., and Ikehara, M. (1991) Importance of the positive charge cluster in *Escherichia coli* ribonuclease HI for the effective binding of the substrate, *J. Biol. Chem. 266*, 11621−11627.
52. Robic, S., Guzman-Casado, M., Sanchez-Ruiz, J. M., and Marqusee, S. (2003) Role of residual structure in the unfolded state of a thermophilic protein, *Proc. Natl. Acad. Sci. U.S.A. 100*, 11345−11349.
53. Karshikoff, A., and Ladenstein, R. (2001) Ion pairs and the thermotolerance of proteins from hyperthermophiles: a "traffic rule" for hot roads, *Trends Biochem. Sci. 26*, 550−556.
54. Lebbink, J. H., Consalvi, V., Chiaraluce, R., Berndt, K. D., and Ladenstein, R. (2002) Structural and thermodynamic studies on a salt-bridge triad in the NADP-binding domain of glutamate dehydrogenase from *Thermotoga maritima*: cooperativity and electrostatic contribution to stability, *Biochemistry 41*, 15524−15535.
55. Schumann, J., Bohm, G., Schumacher, G., Rudolph, R., and Jaenicke, R. (1993) Stabilization of creatinase from *Pseudomonas putida* by random mutagenesis, *Protein Sci. 2*, 1612−1620.
56. Russell, R. J., Hough, D. W., Danson, M. J., and Taylor, G. L. (1994) The crystal structure of citrate synthase from the thermophilic archaeon, *Thermoplasma acidophilum*, *Structure 2*, 1157−1167.
57. Thompson, M. J., and Eisenberg, D. (1999) Transproteomic evidence of a loop-deletion mechanism for enhancing protein thermostability, *J. Mol. Biol. 290*, 595−604.
58. Berezovsky, I. N., and Shakhnovich, E. I. (2005) Physics and evolution of thermophilic adaptation, *Proc. Natl. Acad. Sci U.S.A. 102*, 12742−12747.
59. Ausili, Ausili, A., Cobucci-Ponzano, B., Di Lauro, B., D'Avino, R., Perugino, G., Bertoli, E., Scire, A., Rossi, M., Tanfani, F., and Moracci, M. (2007) A comparative infrared spectroscopic study of glycoside hydrolases from extremophilic archaea revealed different molecular mechanisms of adaptation to high temperatures, *Proteins: Struct., Funct., Bioinf. 67*, 991−1001.
60. Tanaka, T., Sawano, M., Ogasahara, K., Sakaguchi, Y., Bagautdinov, B., Katoh, E., Kuroishi, C., Shinkai, A., Yokoyama, S., and Yutani, K. (2006) Hyper-thermostability of CutA1 protein, with a denaturation temperature of nearly 150 degrees C, *FEBS Lett. 580*, 4224−4230.
61. Huang, H., Chopra, R., Verdine, G. L., and Harrison, S. C. (1998) Structure of a covalently trapped catalytic complex of HIV-1 reverse transcriptase: implications for drug resistance, *Science 282*, 1669−1675.

BI700830F